

Geophysical Research Letters

RESEARCH LETTER

10.1029/2020GL088432

Key Points:

- Juno observes wave and particle phenomena associated with Io's auroral footprint
- Alfvénic acceleration was indicated by observations of magnetic turbulence and broadband electron distributions
- Intense ion cyclotron and whistler-mode radiations are related to auroral ions and electrons, respectively

Supporting Information:

- Supporting Information S1
- Figure S1

Correspondence to:

A. H. Sulaiman,
 ali-sulaiman@uiowa.edu

Citation:





















Sulaiman, A. H., Hospodarsky, G. B., Elliott, S. S., Kurth, W. S., Gurnett, D. A., Imai, M., et al. (2020). Wave-particle interactions associated with Io's auroral footprint: Evidence of Alfvén, ion cyclotron, and whistler modes. *Geophysical Research Letters*, 47, e2020GL088432. <https://doi.org/10.1029/2020GL088432>

Received 15 APR 2020

Accepted 23 JUL 2020

Accepted article online 6 AUG 2020

Wave-Particle Interactions Associated With Io's Auroral Footprint: Evidence of Alfvén, Ion Cyclotron, and Whistler Modes

A. H. Sulaiman¹ , G. B. Hospodarsky¹ , S. S. Elliott¹ , W. S. Kurth¹ , D. A. Gurnett¹ , M. Imai¹ , F. Allegrini^{2,3} , B. Bonfond⁴ , G. Clark⁵ , J. E. P. Connerney^{6,7} , R. W. Ebert^{2,3} , D. J. Gershman⁷ , V. Hue² , S. Janser⁸ , S. Kotsiaros⁹ , C. Paranicas⁵ , O. Santolík^{10,11} , J. Saur⁸ , J. R. Szalay¹² , and S. J. Bolton² 

¹Department of Physics and Astronomy, University of Iowa, Iowa City, IA, USA, ²Southwest Research Institute, San Antonio, TX, USA, ³Department of Physics and Astronomy, University of Texas at San Antonio, San Antonio, TX, USA, ⁴Space Sciences, Technologies and Astrophysics Research Institute, LPAP, Université de Liège, Liège, Belgium, ⁵Applied Physics Laboratory, Johns Hopkins University, Laurel, MD, USA, ⁶Space Research Corporation, Annapolis, MD, USA, ⁷NASA/Goddard Space Flight Center, Greenbelt, MD, USA, ⁸Institute of Geophysics and Meteorology, University of Cologne, Cologne, Germany, ⁹DTU-Space, Technical University of Denmark, Kongens Lyngby, Denmark, ¹⁰Department of Space Physics, Institute of Atmospheric Physics of the Czech Academy of Sciences, Prague, Czechia, ¹¹Faculty of Mathematics and Physics, Charles University, Prague, Czechia, ¹²Department of Astrophysical Sciences, Princeton University, Princeton, NJ, USA

Abstract The electrodynamic coupling between Io and Jupiter gives rise to wave-particle interactions across multiple spatial scales. Here we report observations during Juno's 12th perijove (PJ) high-latitude northern crossing of the flux tube connected to Io's auroral footprint. We focus on plasma wave measurements, clearly differentiating between magnetohydrodynamic (MHD), ion, and electron scales. We find (i) evidence of Alfvén waves undergoing a turbulent cascade, suggesting Alfvénic acceleration processes together with observations of bi-directional, broadband electrons; (ii) intense ion cyclotron waves with an estimated heating rate that is consistent with the generation of ion conics reported by Clark et al. (2020, <https://doi.org/10.1029/2020GL090839>); and (iii) whistler-mode auroral hiss radiation excited by field-aligned electrons. Such high-resolution wave and particle measurements provide an insight into satellite interactions in unprecedented detail. We further anticipate that these spatially well-constrained results can be more broadly applied to better understand processes of Jupiter's main auroral oval.

1. Introduction

Juno is the first spacecraft dedicated to exploring Jupiter's aurora and polar magnetosphere (Bagenal et al., 2017). A payload of high-resolution instruments and the unique spatial coverage enabled by polar orbits afford in situ measurements suited to probe satellite-magnetosphere interactions by sampling magnetic field lines connected to the orbits of the Galilean moons.

First models of the Io footprint assumed that Alfvén waves generated at Io would propagate to Jupiter and back at a time scale lower than that of the plasma convection across Io, thereby establishing a steady-state interaction (Goldreich & Lyndel-Bell, 1969). However, the discovery of the dense Io plasma torus suggested that the Alfvén waves propagate too slowly to return back to Io after partial reflections at the density gradients of the torus boundaries on the Jovian ionosphere (Goertz, 1980; Neubauer, 1980). Analyses of the Io UV footprint morphology indicated that the electron acceleration leading to the aurora should be both bidirectional and broadband (Bonfond et al., 2008, 2009), and subsequent theoretical modeling by Hess et al. (2010) demonstrated that such acceleration occurs at high latitudes by a turbulent cascade of Alfvén waves. Moreover, broadband energy distributions found in the Io footprint tail (Szalay et al., 2018, 2019) suggested continued Alfvénic interaction downstream of Io (Bonfond et al., 2017; Jacobsen et al., 2010; Mura et al., 2018). Similar distributions in Ganymede's footprint tail further reinforce the conclusion that Alfvénic interactions sustain satellite-magnetosphere coupling well into the downstream region (Szalay, Allegrini, et al., 2020).

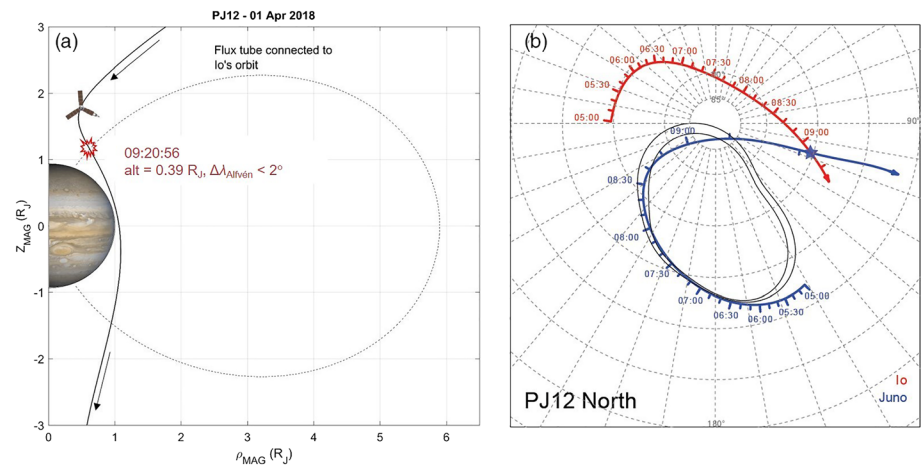


Figure 1. (a) Position of Juno during the PJ12 northern pass with the M-shell connected to Io's orbit overlaid on $\rho_{\text{MAG}} - Z_{\text{MAG}}$ space; where $\rho_{\text{MAG}} = (X_{\text{MAG}}^2 + Y_{\text{MAG}}^2)^{1/2}$, Z_{MAG} is aligned with Jupiter's magnetic dipole, Y_{MAG} is aligned with the intersection of the magnetic and jovigraphic equators, and X_{MAG} completes the right handed system. An M-shell is the magnetic shell for nondipolar magnetic fields (McIlwain, 1961) (b) Polar plot illustrating the magnetic footprints of Juno (blue), Io (red), and the statistical location of Jupiter's main auroral emission (black) (Bonfond et al., 2012) projected onto the Northern Hemisphere as viewed from above.

More broadly, recent works have brought the role of Alfvén, as well as whistler-mode, waves to the fore by invoking their activity to explain the widely observed broadband, precipitating electron energy distributions and accelerated ion populations linked to Jupiter's main auroral emissions (Allegrini et al., 2017, 2020; Damiano et al., 2019; Elliott et al., 2020; Gershman et al., 2019; Kurth et al., 2018; Mauk et al., 2017a, 2017b, 2018).

In this letter, we report high-resolution wave and particle observations during Juno's northern transit of Io's auroral flux tube—likely the Main Alfvén Wing (MAW)—on 1 April 2018 (Szalay et al., 2020). Plasma waves associated with multiple physical scales are detected, and we identify them as Alfvén, ion cyclotron, and whistler modes. The emissions were captured for the first time at Jupiter's high-latitude environment, revealing the large spatial extent of Io's influence in the context of wave-particle processes operating in Jupiter's magnetosphere. We further provide evidence of magnetic turbulence and bidirectional and broadband electrons and demonstrate how the observed waves and satellite auroral particles are intimately linked.

2. Wave and Particle Observations

The primary data set was recorded by the Juno/Waves instrument, which measures an electric field component, E_y , using a 4.8-m tip-to-tip electric dipole antenna oriented along the spacecraft's y axis and contained in its spin (x - y) plane. A magnetic search coil, B_z , has a single sensor parallel to the spacecraft's spin (z) axis. We utilize data provided by the low-frequency receivers, which cover frequency ranges of 50 Hz to 20 kHz (E and B) and 10–150 kHz (E only) with sample rates of 50 and 375 kilosamples per second, respectively. This ensemble further provides the capability of differentiating between electrostatic ($\delta E \gg c\delta B$) and electromagnetic ($\delta E \sim c\delta B$) waves. More details on the Waves instrument, particularly a schematic of the sensors' arrangements, can be found in Kurth et al. (2017).

Juno's position during the PJ12 northern transit of the Io flux tube is illustrated in Figure 1 with the M-shell associated with Io's orbit overlaid in (a) $\rho_{\text{MAG}} - Z_{\text{MAG}}$ space and (b) projected onto the northern polar region as viewed from above using the JRM09 magnetic field model (Connerney et al., 2018) with a current sheet model (Connerney et al., 1981). The angular separation along Io's orbit between Io and an Alfvén wave trajectory connected to Juno's footprint was $< 2^\circ$ —the smallest separation thus far in the mission (Szalay et al., 2020). This event was at the ionospheric end of the flux tube at an altitude of $0.39 R_J$ ($1 R_J = 71,492$ km; Jovian equatorial radius) above the 1-bar level surface. Figure 2 presents a set of time series during this event: Figures 2a and 2b are stacked electric field frequency-time spectrograms from two

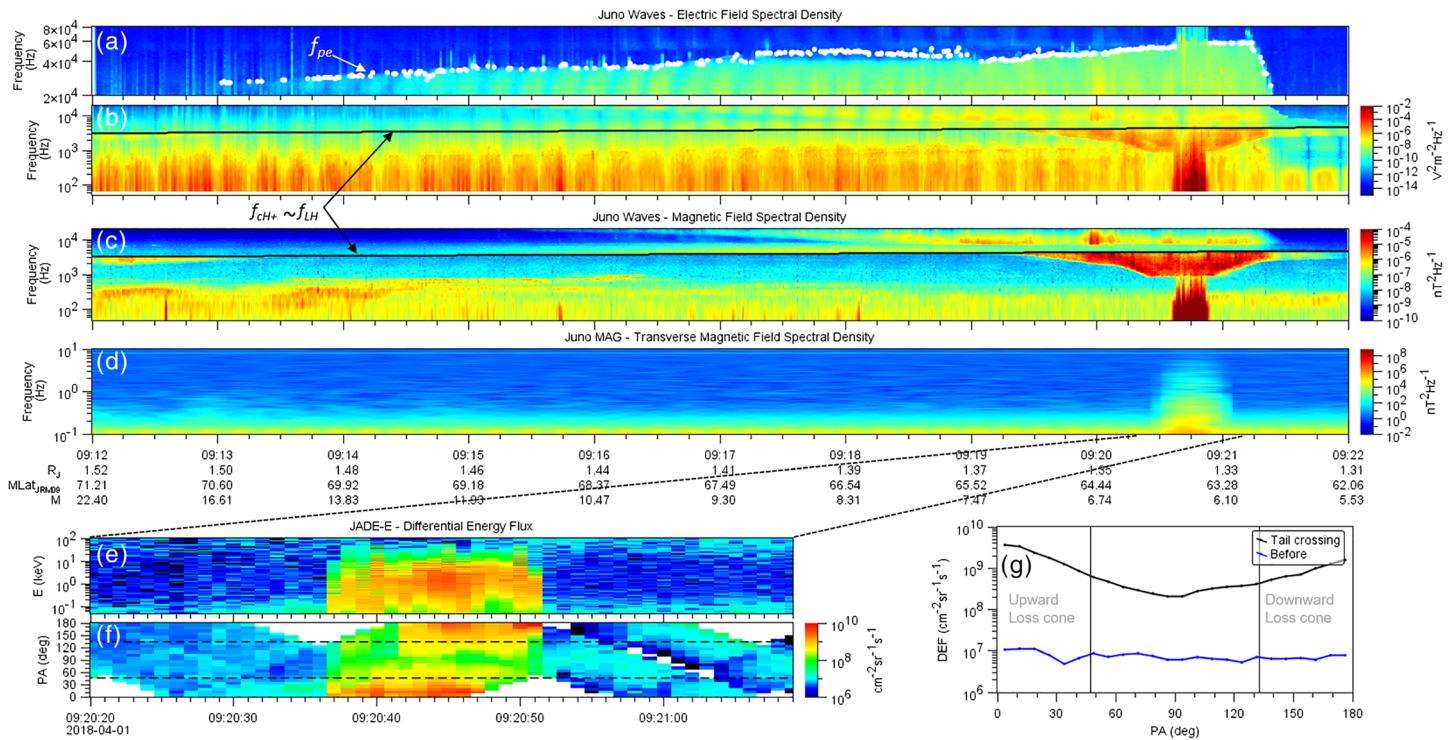


Figure 2. Field and particle observations during Juno's PJ12 northern pass. (a, b) Stacked electric field frequency-time spectrograms. The white trace labeled f_{pe} is the electron plasma frequency as the upper cutoff of the broadband whistler-mode waves, noting the electron cyclotron frequency is much higher, that is, upper cutoff frequency equals $\min\{f_{pe}, f_{ce}\}$. (c, d) Stacked magnetic field frequency-time spectrograms recorded by Waves and MAG, respectively. The black solid line represents the proton cyclotron frequency derived from MAG. (e) Electron differential energy flux (DEF) energy-time and (f) pitch angle-time spectrograms. (g) Electron DEF versus pitch angles during the tail crossing at 09:20:44 (black) and before (blue).

channels covering continuously a frequency range of 50 Hz to 80 kHz; Figures 2c and 2d are stacked (transverse) magnetic field frequency-time spectrograms from the magnetic search coil and fluxgate magnetometer (MAG) (Connerney et al., 2017), respectively, covering a frequency range of 0.2 Hz to 20 kHz (not continuous across instruments); Figures 2e and 2f are the energy-time and pitch angle-time electron differential energy flux, respectively, recorded by the Jovian Auroral Distributions Experiment (JADE-E) (McComas et al., 2017) covering an energy range of 50 eV to 100 keV for 49 s during the flux tube crossing; Figure 2g compares the pitch angle distributions during the Io flux tube crossing at 09:20:44 and the background. Calculated from MAG and overlaid on the frequency-time spectrograms is the proton cyclotron frequency, f_{ch+} , revealing that the Waves instrument is sensitive to plasma wave phenomena well within subproton scales by virtue of Jupiter's strong magnetic field.

3. Interpretation and Discussion

3.1. Plasma Waves Below f_{ch+} : Alfvénic Turbulence and Ion Cyclotron Heating

We begin with waves in the lower frequency range below f_{ch+} . The emissions in this range are the most intense both in electric and magnetic field spectral densities, as shown in Figures 2b and 2c. Using MAG, Gershman et al. (2019) transformed magnetic field fluctuations into compressive and noncompressive (transverse) components. During passes of Jupiter's aurora, they found the power of the fluctuations predominantly in the transverse component between 0.2 and 5 Hz (frequency range was limited by noise). These were identified as Alfvénic turbulence, and their activity was pronounced during Io footprint tail crossings at longitudinal separations up to 90°.

On first inspection of the magnetic search coil data, it appears that the “stem” between 50 and ~800 Hz and at 09:20:35–09:20:54 in Figure 2c is an extension of the Alfvénic activity identified by MAG in Figure 2d. This can be tested by exploiting the orientation of the Waves instrument on the spacecraft with respect to the

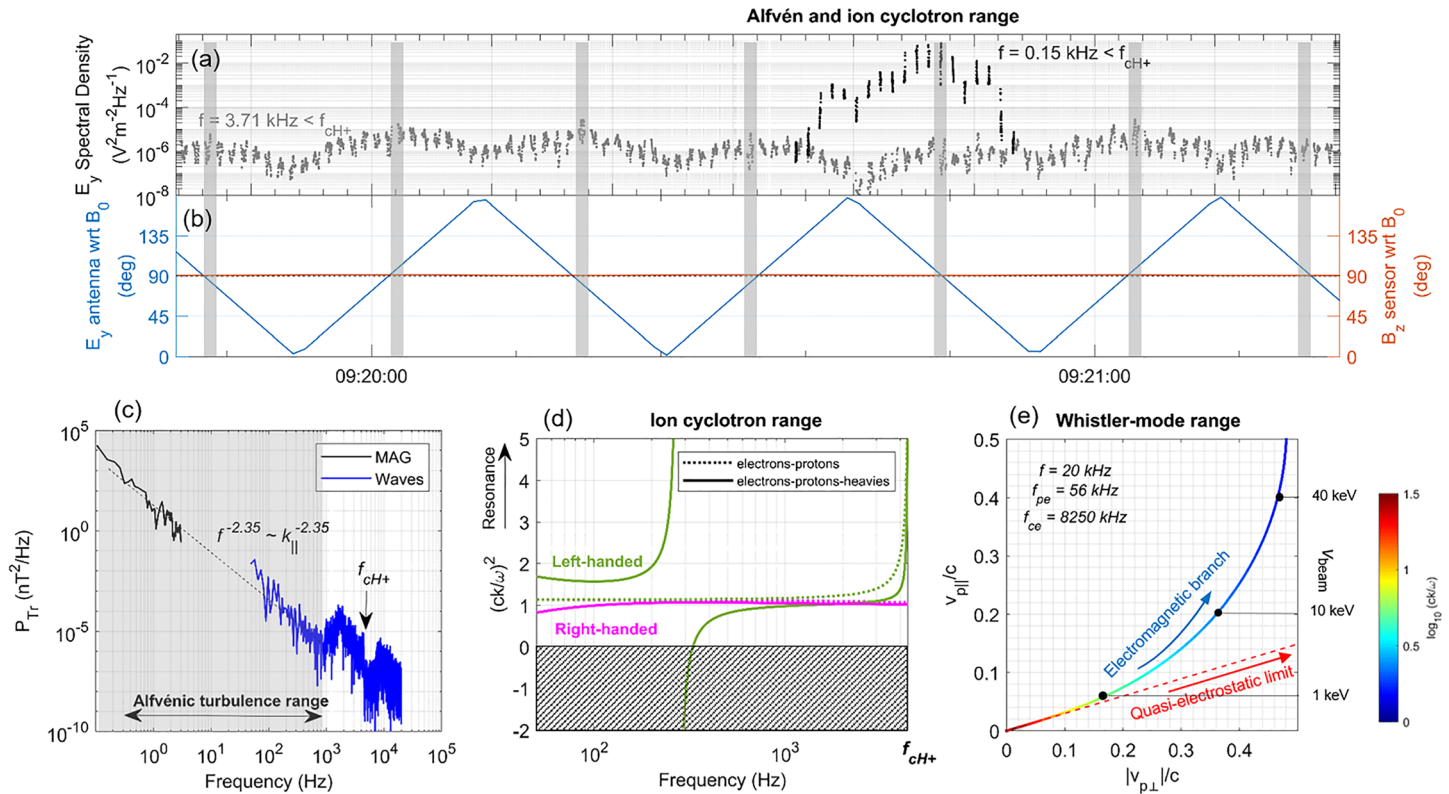


Figure 3. Plasma wave diagnosis across different scales. (a) E_y spectral densities at 0.15 and 3.71 kHz, modulated by the spacecraft spin period. (b) Angle between E_y and \vec{B}_0 (blue) and angle between B_z and \vec{B}_0 (red). (c) Combined power spectral densities of the measured transverse magnetic field fluctuations by MAG (black) and Waves (blue) covering a large range in Alfvén frequency space. (d) Dispersion relations of left-hand and right-hand polarized modes plotted as index of refraction versus frequency up to f_{cH+} . The hatched area is the region of evanescence, and outside is the region of propagation. (e) Solutions of the whistler-mode dispersion relation on phase velocity space color-coded by their corresponding index of refraction, ck/ω . The parallel phase speeds of the whistler-mode wave (left y axis) can be related to the electron beam speed (right y axis) through the Landau resonance condition $v_{p\parallel} \approx v_{beam}$.

background magnetic field. The effective axis of the electric field antenna in the spin plane induces modulations in E_y at half the spacecraft spin period of 30 s. The spacecraft attitude was such that the spin axis was approximately perpendicular to a Jovian magnetic meridian plane. This fortuitous configuration meant that the E_y axis measured electric field fluctuations parallel and perpendicular to the background magnetic field, \vec{B}_0 , and therefore the twice-per-spin peaks can be correlated with projections of E_y on \vec{B}_0 . At the same time, the B_z axis of the search coil measured magnetic field fluctuations purely perpendicular to \vec{B}_0 . Figure 3a shows the modulations of E_y spectral densities in the range below f_{cH+} ($f = 0.15$ and 3.71 kHz), where Alfvén and ion cyclotron waves can propagate, and Figure 3b shows the angles of E_y (blue) and B_z (red) with respect to \vec{B}_0 . It is clear that the E_y spectral density peaks near $E_y \perp \vec{B}_0$ and depresses near $E_y \parallel \vec{B}_0$. This pattern holds for any frequency in this range and is consistent with transverse electric field fluctuations of Alfvén and ion cyclotron waves. Furthermore, we have continuous $B_z \perp \vec{B}_0$, meaning that the wave emissions from the search coil (Figure 2c) can indeed be interpreted as an extension of the transverse MAG fluctuations (Figure 2d) in frequency space. Based on the spacecraft speed, transit time, and correcting for the oblique angle at which Juno crosses the flux tube, the estimated transverse length scale of the flux tube is $\sim 1,000 \pm 50$ km.

Figure 3c combines power spectral densities of the measured transverse magnetic field fluctuations from both MAG and Waves. Interestingly, both frequency ranges can be connected by a power law of spectral index -2.35 ± 0.07 up to ~ 800 Hz. The semirelativistic Alfvén speed at high latitudes compared to the spacecraft speed of 51 km/s makes the effect of Doppler shift negligible; therefore, the measured fluctuations can be considered to be in the plasma frame. As indicated by Gershman et al. (2019), the dispersion relation in

the semirelativistic Alfvén wave limit, that is, $\omega/k_{\parallel} \sim c$, means that the spectral index is equivalent to a turbulent cascade in k_{\parallel} , rather than in k_{\perp} which is typically discussed in the context of Alfvénic turbulence (e.g., Chaston et al., 2008; Saur et al., 2018), where k is the wavenumber and $\omega = 2\pi f$ is the angular frequency. That said, Gershman et al. (2019) invoked partially developed critically balanced Kolmogorov cascade as a possible explanation for their resolved scaling of $k_{\parallel}^{-2.29 \pm 0.09}$ (0.2–5 Hz) associated with the main auroral emission at Jupiter’s high latitudes. This type of cascade exhibits perpendicular and parallel spectral indices of $-5/3$ and -2 , respectively. The resolved scaling of $k_{\parallel}^{-2.35 \pm 0.07}$ for the Io auroral flux tube is consistent with that of the main auroral emission suggesting a similar auroral mechanism.

Further, the calculated Poynting flux was $\sim 3,000$ mW/m² associated with the frequency range of 0.2–5 Hz (Gershman et al., 2019). We band-pass-filtered multiple waveform snapshots between 50 and 800 Hz, and the calculated root mean squares, δB , were in the range ~ 1 –2 nT. This corresponds to Poynting fluxes, $\delta B^2 c / \mu_0$, of ~ 0.2 –1 mW/m² associated with magnetic field fluctuations that cascaded to scales in the range 50–800 Hz. Using this relation, for the frequency range between 0.2 and 800 Hz, the corresponding parallel wavelengths are cascaded from ~ 20 to $10^{-3} R_J$. These Alfvénic magnetic signatures together with measurements of broadband precipitating electron fluxes in Figure 2e are also a characteristic feature of Alfvénic acceleration associated with footprint tail aurorae (Szalay, Allegrini et al., 2020; Szalay et al., 2018).

Since the magnetohydrodynamic (MHD) Alfvén wave propagates parallel to the magnetic field, it follows that the time of its detection is coincident with the time of the Io flux tube transit at 09:20:35–09:20:54. A dispersive feature becomes present above ~ 800 Hz and up to f_{cH+} , where higher frequencies are detected at times before and after the Io flux tube crossing, thereby displaying a “funnel” spectral feature. This is characteristic of plasma wave propagation along the resonance cone.

Figure 3d plots the indices of refraction, ck/ω , as a function of frequency for parallel-propagating right-hand and left-hand polarized modes as

$$\left(\frac{ck}{\omega}\right)_{R,L}^2 = 1 - \sum_s \frac{f_{ps}^2}{f(f \pm f_{cs})} \quad (1)$$

where f_p and f_c are the plasma and cyclotron frequencies, respectively, and the subscript s denotes the species. The right-hand (R) and left-hand (L) polarized modes take the “+” and “–” signs, respectively, noting that f_c is negative for electrons (Gurnett & Bhattacharjee, 2017). For each mode, the dispersion relations are derived for an electron-proton plasma and another with added 10% S²⁺ and 10% O⁺ by composition. Note that these compositions are not derived from data as their same mass-to-charge ratios makes it difficult to separate their time-of-flight effects. They are merely to show that the inclusion of heavies changes the spectral character and yields an additional resonance at a lower cyclotron frequency for the left-handed mode, where $(ck/\omega)^2$ goes to infinity. However, this frequency is the same for S²⁺ and O⁺ at ~ 270 Hz and does not explain the distinct spectral feature at ~ 800 Hz. It is worth noting that the lower frequencies in the Alfvén range do not necessarily continuously connect through to f_{cH+} . Since a characteristic frequency existing below f_{cH+} (e.g., an ion hybrid frequency) requires additional species to an electron-proton plasma, we conclude that the distinct feature at ~ 800 Hz and the resonance cone above is strongly suggestive of the presence of heavies. Modeling efforts will be required (Santolík et al., 2016) once the heavy ions compositions are available to fully resolve the spectral significance at ~ 800 Hz.

For both plasmas, the left-handed modes undergo resonance at f_{cH+} , indicating that the observed intense plasma waves exhibiting a significant drop in power at f_{cH+} are left handed. This signifies strong interactions with protons as they rotate in the same left-hand sense as the wave electric field. These emissions are consistent with the ion cyclotron mode and can, in theory, set up a resonance leading to efficient ion energization at a Doppler-shifted frequency that matches the cyclotron frequency of an ion (e.g., André et al., 1998; Chang et al., 1986; Lysak, 1986). This wave-particle interaction is likely responsible for the anti-planetward transport of thermal ions along diverging magnetic field lines, resulting in an ion conic distribution in velocity space observed during this Io event (Clark et al., 2020), representing the first observation of this kind in a moon-magnetosphere context. Such distributions are commonly observed at Earth (Carlson et al., 1998) and have been reported at Saturn (Mitchell et al., 2009).

Assuming all the wave power in this frequency range up to f_{cH+} resides in the left-hand mode, the maximum ion cyclotron heating rate can be estimated, as derived by Chang et al. (1986):

$$\frac{dW_{\perp, \text{res}}}{dt} = \frac{S_E q^2}{2m_p} \quad (2)$$

where q and m_p are the charge and mass of a proton, respectively. A (maximum) electric field spectral density, S_E , at f_{cH+} measured at $\sim 10^{-5} \text{ V}^2\text{m}^{-2} \text{ Hz}^{-1}$ will yield a heating rate of $\sim 500 \text{ eV/s}$. Note that an exact calculation of the heating rate would require knowledge of the fraction of waves near f_{cH+} that are both left-handed and resonating with ions; therefore, this may be considered as an upper limit. Together with the high-energy particle observations reported by Clark et al. (2020), there appears to be a causal link between these observed ion cyclotron waves and the ion conic distributions since (i) the observed ion energies on the order of 10–100 keV at low altitudes are consistent with the estimated heating rate along their travel path between the source and the spacecraft, suggesting that a large fraction of these waves are in resonance with the ions, and (ii) both the waves and the ions are found to be propagating upward from Jupiter (the wave propagation direction is shown in Figure S1 in the supporting information).

3.2. Plasma Waves Above f_{cH+} : Beam-Plasma Instability

Next, we explore the higher frequency range belonging to the electron scale. The most apparent emission is the larger V-shaped spectral feature between 09:13 and 09:22, between f_{cH+} and a sharp upper frequency cutoff marked by the white trace and labeled f_{pe} , in Figures 2a–2c. This is characteristic of a whistler-mode auroral hiss emission. This class of plasma wave emissions is understood to be generated by a coherent beam-plasma instability (Maggs, 1989) at the Landau resonance. Here, the parallel phase speed of the wave almost matches the electron beam speed, $\omega/k_{\parallel} \approx v_{\text{beam}}$. Since electron beams provide the free energy for their growth, they are typically observed in the presence of field-aligned currents such as in the auroral regions of Earth (James, 1976), Saturn (Gurnett et al., 2011), and Jupiter (Tetrack et al., 2017). Auroral hiss emissions are therefore diagnostics of electrodynamic coupling between conductive bodies and have been observed widely in Saturn's magnetosphere. The Cassini spacecraft observed their presence on magnetic flux tubes connected to Enceladus (Gurnett et al., 2011; Sulaiman, Kurth, Hospodarsky, Averkamp, Ye, et al., 2018) coincident with field-aligned currents and, surprisingly, connected to Saturn's main rings (Sulaiman, Kurth, Hospodarsky, Averkamp, Persoon, et al., 2018, 2019; Xin et al., 2006).

The propagation of whistler-mode auroral hiss along the resonance cone has a dispersion relation that goes as $\sin \psi_{\text{res}} \approx f/f_{pe}$ (Gurnett et al., 1983). This is a special case in a highly magnetized regime descriptive of the near-Jupiter environment, that is, $f_{ce}^2 \gg f_{pe}^2$, where f_{ce} and f_{pe} are the electron cyclotron and plasma frequencies, respectively. It follows that at lower frequencies, f , the ray path (or group velocity) angles, ψ_{res} , are more parallel to the magnetic field and become monotonically more perpendicular with higher frequencies. This explains the V-shaped “funnel” feature on the spectrograms in Figures 2a–2c as higher frequencies are detected farther away from the Io flux tube. The dispersion relation holds up to a maximum $f = f_{pe}$, which corresponds to the upper frequency cutoff in Figure 2a. Using this technique, the electron number density, n_e , can be derived as $f_{pe} [\text{Hz}] = 8,980\sqrt{n_e [\text{cm}^{-3}]}$. This yields a density in the range of 8–40 cm^{-3} .

We next examine the lower frequency cutoff for the whistler mode, which is the lower hybrid frequency, f_{LH} . This is achieved by numerically solving for the hybrid resonances at $S = 0$, where S is the appropriate element in the cold magnetized plasma dielectric tensor as defined by Stix (1992). This is given by

$$S = 1 - \sum_s \frac{f_{ps}^2}{f^2 - f_{cs}^2} = 0 \quad (3)$$

with the subscript s denoting the species. Assuming a quasi-neutral plasma of electrons and protons, in this highly magnetized regime where $f_{ce}/f_{pe} \sim O(10^2)$, the solution yields $f_{LH} \approx f_{cH+}$. Contributions from O^+ and S^{2+} are negligible as their comparatively large mass-to-charge ratios will act to only slightly reduce f_{LH} . Note this regime is exceptionally highly magnetized and in contrast to the magnetized regimes considered near Earth and Saturn, commonly approximated as $f_{LH} \approx f_{pH+}$, where f_{pH+} is the proton plasma

frequency (e.g., Sulaiman et al., 2017). The significance of identifying f_{LH} is that it represents the surface at which the wave normal angles of the whistler mode rotate through 90° and are reflected. In other words, the frequencies are not continuous across $f_{cH+}(\approx f_{LH})$, thereby decoupling the whistler mode from the intense wave emissions below f_{cH+} in Figures 2b and 2c.

For the whistler-mode auroral hiss to grow, an electron beam is required to provide the free energy, and this explains the contemporaneous observations with field-aligned electrons as detected by JADE (Figures 2f and 2g). The waves are amplified via Landau resonance where the parallel phase speed ω/k_{\parallel} almost matches the beam speed v_{beam} . The JADE-E instrument measured upward and downward field-aligned electron populations in the range 50 eV to 30 keV. To relate these energies to the observed whistler-mode auroral hiss, we consider the dispersion relation for waves in a cold collisionless plasma (Stix, 1992). The special case for electron scales is known as the Appleton-Hartree equation and is given by

$$\left(\frac{ck}{\omega}\right)^2 = 1 - \frac{X(1-X)}{1 - X - \frac{1}{2}Y^2\sin^2\theta \pm \left(\left(\frac{1}{2}Y^2\sin^2\theta\right)^2 + (1-X)^2Y^2\cos^2\theta\right)^{\frac{1}{2}}} \quad X = \frac{f_{pe}^2}{f^2} \text{ and } Y = \frac{f_{ce}}{f} \quad (4)$$

where θ is the angle between the magnetic field and the wave vector \vec{k} . The reciprocal of the calculated index of refraction from Equation 4 can be related to electron energy via the Landau resonance condition, that is, $\omega/ck_{\parallel} \equiv v_{p\parallel}/c \approx v_{\text{beam}}/c$, where v_p is the phase speed. Figure 3e shows the set of solutions in phase velocity space for which the whistler mode can exist, given the plasma properties during the Io flux tube crossing. The solutions can be classified into two parts: (i) points that lie on the quasi-electrostatic limit (low $v_{p\parallel}/c$) characterized by higher indices of refraction and (ii) points that depart from this limit are in the electromagnetic branch (high $v_{p\parallel}/c$). Taking the electron energy measured at 1 keV yields $v_{\text{beam}}/c = 0.063$, and the equivalent $v_{p\parallel}/c$ on Figure 3e intersects a solution on the curve that just departed from the quasi-electrostatic limit. Higher electron energies, such as 10 keV and above, place the solution well within the electromagnetic branch. Measured $\delta E/c\delta B \gtrsim 1$ of the whistler-mode auroral hiss (Figures 2a–2c) imply an electromagnetic nature, and this is therefore consistent with their generation by electron beams most likely in the 1–30 keV range. Furthermore, quasiparallel propagation of whistler-mode waves excited by a cyclotron resonance could partly account for the observed electromagnetic nature, as observed in the flux tube of Saturn's moon Rhea (Santolik et al., 2011). However, the observed electron distribution and the funnel-shaped feature of the spectrogram make this unlikely.

In contrast, auroral hiss emissions observed by Cassini on the Enceladus flux tube were purely electrostatic (i.e., $\delta E/c\delta B \gg 1$) and observed in the presence of electron beams up to 10 eV (=very low $v_{p\parallel}/c$), thus placing the solution well within the quasi-electrostatic limit (Gurnett et al., 2011; Sulaiman, Kurth, Hospodarsky, Averkamp, Ye, et al., 2018). By this association, auroral hiss observations may be used to constrain electron energies where particle observations are not available.

The Landau resonance condition, for the generation of whistler-mode auroral hiss, requires both waves and particles traveling in the same direction. Since the observed Poynting flux is upgoing (Figure S1), we can then infer that the whistler-mode auroral hiss emissions are associated with the upgoing electron population, that is, pitch angle $\approx 0^\circ$ (Figure 2f). Enhanced whistler-mode radiation has been reported in Io's wake by Paranicas et al. (2019), where they suggested, consistent with modeling, that wave-particle interaction plays a key role in the simultaneously observed depletions of energetic ions and electrons. Such signatures were not observed during this pass, and this highlights the complexity of wave-particle processes on satellite flux tubes.

4. Conclusions

Fluid-scale perturbations near the satellites give rise to Alfvén waves, which act to transmit the field-aligned currents driven by the motion of Io through the dense magnetized plasma of Jupiter's magnetosphere. Wave-particle interaction is understood to be achieved when these Alfvén waves nonlinearly interact with their reflected counterparts, undergoing a turbulent cascade from large to small spatial and temporal scales (Hess et al., 2010; Saur et al., 2002). At sufficiently small scales, the waves and particles are able to

exchange energy, thereby accelerating and heating auroral particles fueled by converted electromagnetic energy (Saur et al., 2018). Since particle energization is characterized by distortions in phase space, the particle distributions become unstable to plasma waves which can, in turn, act to scatter particles.

We have presented field and particle observations during Juno's PJ12 crossing of the Io's flux tube, likely the Main Alfvén Wing, and showed how they are related in the context of wave-particle processes of a moon-magnetosphere interaction. Our conclusions are the following:

1. Identification of Alfvénic magnetic turbulence across a large frequency range. This observation, in concert with broadband precipitating electron fluxes, underlines Alfvénic acceleration as Jupiter's primary auroral mechanism, as observed throughout the main and satellite footprint tail aurorae by numerous works.
2. A commonly proposed mechanism for ion energization is the ion cyclotron resonance. Left-hand polarized ion cyclotron waves were identified, and it is likely that these are responsible for transversely heated upwelling ions that develop into ion conic distributions, as reported by Clark et al. (2020).
3. A field-aligned electron population is unstable to the generation of whistler-mode auroral hiss. From the Landau resonance condition, we related the electromagnetic nature of the whistler-mode with observed upward electron beams in the order of 1 keV. In contrast, an analogous quasi-electrostatic observation on the Saturn-Enceladus flux tube by Cassini was shown to be associated with energies in the order of 1 eV (Sulaiman, Kurth, Hospodarsky, Averkamp, Ye, et al., 2018).

Data Availability Statement

The Waves, JADE, and MAG data used in this article have the Dataset ID JNO-E/J/SS-WAV-3-CDR-BSTFULL-V1.0, JNO-J/SW-JAD-3-CALIBRATED-V1.0, and JNO-J-3-FGM-CAL-V1.0, respectively, and are publicly accessible through the Planetary Plasma Interactions Node in the Planetary Data System (<https://pds-ppi.igpp.ucla.edu/>). In this paper, we use an effective E-field antenna length of 0.5 m.

Acknowledgments

The authors gratefully acknowledge J. Faden and the use of Autoplot. The research at the University of Iowa was supported by NASA through Contract 699041X with the Southwest Research Institute. O. S. acknowledges support from the LTAUSA17070 project and from the Praemium Academiae Award.

References

- Allegrini, F., Bagenal, F., Bolton, S., Connerney, J., Clark, G., Ebert, R. W., et al. (2017). Electron beams and loss cones in the auroral regions of Jupiter. *Geophysical Research Letters*, *44*, 7131–7139. <https://doi.org/10.1002/2017GL073180>
- Allegrini, F., Mauk, B., Clark, G., Gladstone, G. R., Hue, V., Kurth, W. S., et al. (2020). Energy flux and characteristic energy of electrons over Jupiter's main auroral emission. *Journal of Geophysical Research: Space Physics*, *125*, e2019JA027693. <https://doi.org/10.1029/2019JA027693>
- André, M., Norqvist, P., Andersson, L., Eliasson, L., Eriksson, A. I., Blomberg, L., et al. (1998). Ion energization mechanisms at 1700 km in the auroral region. *Journal of Geophysical Research*, *103*(A3), 4199–4222. <https://doi.org/10.1029/97JA00855>
- Bagenal, F., Adriani, A., Allegrini, F., Bolton, S. J., Bonfond, B., Bunce, E. J., et al. (2017). Magnetospheric science objectives of the Juno mission. *Space Science Reviews*, *213*(1–4), 219–287. <https://doi.org/10.1007/s11214-014-0036-8>
- Bonfond, B., Grodent, D., Gérard, J. C., Radioti, A., Dols, V., Delamere, P. A., & Clarke, J. T. (2009). The Io UV footprint: Location, inter-spot distances and tail vertical extent. *Journal of Geophysical Research*, *114*, A07224. <https://doi.org/10.1029/2009JA014312>
- Bonfond, B., Grodent, D., Gérard, J. C., Radioti, A., Saur, J., & Jacobsen, S. (2008). UV Io footprint leading spot: A key feature for understanding the UV Io footprint multiplicity? *Journal of Geophysical Research*, *35*, L05107. <https://doi.org/10.1029/2007GL032418>
- Bonfond, B., Grodent, D., Gérard, J. C., Stallard, T., Clarke, J. T., Yoneda, M., et al. (2012). Auroral evidence of Io's control over the magnetosphere of Jupiter. *Geophysical Research Letters*, *39*, L01105. <https://doi.org/10.1029/2011GL050253>
- Bonfond, B., Saur, J., Grodent, D., Badman, S. V., Bisikalo, D., Shematovich, V., et al. (2017). The tails of the satellite auroral footprints at Jupiter. *Journal of Geophysical Research: Space Physics*, *122*, 7985–7996. <https://doi.org/10.1002/2017JA024370>
- Carlson, C. W., McFadden, J. P., Ergun, R. E., Temerin, M., Peria, W., Mozer, F. S., et al. (1998). FAST observations in the downward auroral current regions: Energetic upgoing electron beams, parallel potential drops, and ion heating. *Geophysical Research Letters*, *25*(12), 2017–2020. <https://doi.org/10.1029/98GL00851>
- Chang, T., Crew, G. B., Hershkowitz, N., Jasperse, J. R., Retterer, J. M., & Winningham, J. D. (1986). Transverse acceleration of oxygen ions by electromagnetic ion cyclotron resonance with broad band left-hand polarized waves. *Geophysical Research Letters*, *13*(7), 636–639. <https://doi.org/10.1029/GL013i007p00636>
- Chaston, C. C., Salem, C., Bonnell, J. W., Carlson, C. W., Ergun, R. E., Strangeway, R. J., & McFadden, J. P. (2008). The turbulent Alfvénic aurora. *Physical Review Letters*, *100*(17), 175003. <https://doi.org/10.1103/PhysRevLett.100.175003>
- Clark, G., Mauk, B. H., Kollmann, P., Szalay, J. R., Sulaiman, A. H., Gershman, D. J., et al. (2020). Energetic proton conics associated with Io's footprint tail. <https://doi.org/10.1029/2020GL090839>
- Connerney, J. E. P., Acuña, M. H., & Ness, N. F. (1981). Modeling the Jovian current sheet and inner magnetosphere. *Journal of Geophysical Research*, *86*(A10), 8370–8384. <https://doi.org/10.1029/JA086iA10p08370>
- Connerney, J. E. P., Benn, M., Bjarno, J. B., Denver, T., Espley, J., Jorgensen, J. L., et al. (2017). The Juno magnetic field investigation. *Space Science Reviews*, *213*(1–4), 39–138. <https://doi.org/10.1007/s11214-017-0334-z>
- Connerney, J. E. P., Kotsiaros, S., Oliverson, R. J., Espley, J. R., Joergensen, J. L., Joergensen, P. S., et al. (2018). A new model of Jupiter's magnetic field from Juno's first nine orbits. *Geophysical Research Letters*, *45*, 2590–2596. <https://doi.org/10.1002/2018GL077312>

- Damiano, P. A., Delamere, P. A., Stauffer, B., Ng, C. S., & Johnson, J. R. (2019). Kinetic simulations of electron acceleration by dispersive scale Alfvén waves in Jupiter's magnetosphere. *Geophysical Research Letters*, *46*, 3043–3051. <https://doi.org/10.1029/2018GL081219>
- Elliott, S. S., Gurnett, D. A., Yoon, P. H., Kurth, W. S., Mauk, B. H., Ebert, R. W., et al. (2020). The generation of upward-propagating whistler-mode waves by electron beams in the Jovian polar regions. *Journal of Geophysical Research: Space Physics*, *125*, e27868. <https://doi.org/10.1029/2020JA027868>
- Gershman, D. J., Connerney, J. E. P., Kotsiaros, S., DiBraccio, G. A., Martos, Y. M., Viñas, A. F., et al. (2019). Alfvénic fluctuations associated with Jupiter's auroral emissions. *Geophysical Research Letters*, *46*, 7157–7165. <https://doi.org/10.1029/2019GL082951>
- Goertz, C. K. (1980). Io's interaction with the plasma torus. *Journal of Geophysical Research*, *85*(A6), 2949. <https://doi.org/10.1029/JA085iA06p02949>
- Goldreich, P., & Lyndel-Bell, D. (1969). Io, a Jovian unipolar inductor. *Astrophysical Journal*, *156*, 59–78. <https://doi.org/10.1086/149947>
- Gurnett, D. A., Averkamp, T. F., Schippers, P., Persoon, A. M., Hospodarsky, G. B., Leisner, J. S., et al. (2011). Auroral hiss, electron beams and standing Alfvén wave currents near Saturn's moon Enceladus. *Geophysical Research Letters*, *38*, L06102. <https://doi.org/10.1029/2011GL046854>
- Gurnett, D. A., & Bhattacharjee, A. (2017). *Introduction to plasma physics: With space, laboratory and astrophysical applications* (2nd ed.). Cambridge: Cambridge University Press. <https://doi.org/10.1017/9781139226059>
- Gurnett, D. A., Shawhan, S. D., & Shaw, R. R. (1983). Auroral hiss, Z mode radiation, and auroral kilometric radiation in the polar magnetosphere: DE 1 observations. *Journal of Geophysical Research*, *88*(A1), 329–340. <https://doi.org/10.1029/JA088iA01p00329>
- Hess, S. L. G., Delamere, P., Dols, V., Bonfond, B., & Swift, D. (2010). Power transmission and particle acceleration along the Io flux tube. *Journal of Geophysical Research*, *115*, A06205. <https://doi.org/10.1029/2009JA014928>
- Jacobsen, S., Saur, J., Neubauer, F. M., Bonfond, B., Gérard, J. C., & Grodent, D. (2010). Location and spatial shape of electron beams in Io's wake. *Journal of Geophysical Research*, *115*, A04205. <https://doi.org/10.1029/2009JA014753>
- James, H. G. (1976). VLF saucers. *Journal of Geophysical Research*, *81*(4), 501–514. <https://doi.org/10.1029/JA081i004p00501>
- Kurth, W. S., Hospodarsky, G. B., Kirchner, D. L., Mokrzycki, B. T., Averkamp, T. F., Robison, W. T., et al. (2017). The Juno Waves investigation. *Space Science Reviews*, *213*(1–4), 347–392. <https://doi.org/10.1007/s11214-017-0396-y>
- Kurth, W. S., Mauk, B. H., Elliott, S. S., Gurnett, D. A., Hospodarsky, G. B., Santolik, O., et al. (2018). Whistler mode waves associated with broadband auroral electron precipitation at Jupiter. *Geophysical Research Letters*, *45*, 9372–9379. <https://doi.org/10.1029/2018GL078566>
- Lysak, R. L. (1986). Ion acceleration by wave-particle interaction. *Journal of Geophysical Research*, *38*, 261–270. <https://doi.org/10.1029/GM038p0261>
- Maggs, J. E. (1989). Nonlinear evolution of the auroral electron beam. *Journal of Geophysical Research*, *94*(A4), 3631–3651. <https://doi.org/10.1029/JA094iA04p03631>
- Mauk, B. H., Haggerty, D. K., Paranicas, C., Clark, G., Kollmann, P., Rymer, A. M., et al. (2017a). Discrete and broadband electron acceleration in Jupiter's powerful aurora. *Nature*, *549*, 66–69. <https://doi.org/10.1038/nature23648>
- Mauk, B. H., Haggerty, D. K., Paranicas, C., Clark, G., Kollmann, P., Rymer, A. M., et al. (2017b). Juno observations of energetic charged particles over Jupiter's polar regions: Analysis of mono- and bi-directional electron beams. *Geophysical Research Letters*, *44*, 4410–4418. <https://doi.org/10.1002/2016GL072286>
- Mauk, B. H., Haggerty, D. K., Paranicas, C., Clark, G., Kollmann, P., Rymer, A. M., et al. (2018). Diverse electron and ion acceleration characteristics observed over Jupiter's main aurora. *Geophysical Research Letters*, *45*, 1277–1285. <https://doi.org/10.1002/2017GL076901>
- McComas, D. J., Alexander, N., Allegrini, F., Bagenal, F., Beebe, C., Clark, G., et al. (2017). The Jovian Auroral Distributions Experiment (JADE) on the Juno Mission to Jupiter. *Space Science Reviews*, *213*(1–4), 547–643. <https://doi.org/10.1007/s11214-013-9990-9>
- McIlwain, C. E. (1961). Coordinates for mapping the distribution of magnetically trapped particles. *Journal of Geophysical Research*, *66*(11), 3681–3691. <https://doi.org/10.1029/JZ066i011p03681>
- Mitchell, D. G., Kurth, W. S., Hospodarsky, G. B., Krupp, N., Saur, J., Mauk, B. H., et al. (2009). Ion conics and electron beams associated with auroral processes on Saturn. *Journal of Geophysical Research*, *114*, A02212. <https://doi.org/10.1029/2008JA013621>
- Mura, A., Adriani, A., Connerney, J. E. P., Bolton, S., Altieri, F., Bagenal, F., et al. (2018). Juno observations of spot structures and a split tail in Io-induced aurorae in Jupiter. *Nature*, *361*(6404), 774–777. <https://doi.org/10.1126/science.aat1450>
- Neubauer, F. M. (1980). Nonlinear standing Alfvén wave current system at Io: Theory. *Journal of Geophysical Research*, *85*(A3), 1171–1178. <https://doi.org/10.1029/JA085iA03p01171>
- Paranicas, C., Mauk, B. H., Haggerty, D. K., Clark, G., Kollmann, P., Rymer, A. M., et al. (2019). Io's effect on energetic charged particles as seen in Juno data. *Geophysical Research Letters*, *46*, 13,615–13,620. <https://doi.org/10.1029/2019GL085393>
- Santolik, O., Gurnett, D. A., Jones, G. H., Schippers, P., Crary, F. J., Leisner, J. S., et al. (2011). Intense plasma wave emissions associated with Saturn's moon Rhea. *Geophysical Research Letters*, *38*, L19204. <https://doi.org/10.1029/2011GL049219>
- Santolik, O., Parrot, M., & Němec, F. (2016). Propagation of equatorial noise to low altitudes: Decoupling from the magnetosonic mode. *Geophysical Research Letters*, *43*, 6694–6704. <https://doi.org/10.1002/2016GL069582>
- Saur, J., Janser, S., Schreiner, A., Clark, G., Mauk, B. H., Kollmann, P., et al. (2018). Wave-particle interaction of Alfvén waves in Jupiter's magnetosphere: Auroral and magnetospheric particle acceleration. *Journal of Geophysical Research: Space Physics*, *123*, 9560–9573. <https://doi.org/10.1029/2018JA025948>
- Saur, J., Politano, H., Pouquet, A., & Matthaeus, W. H. (2002). Evidence for weak MHD turbulence in the middle magnetosphere of Jupiter. *Astronomy & Astrophysics*, *386*(2), 699–708. <https://doi.org/10.1051/0004-6361:20020305>
- Stix, T. H. (1992). *Waves in plasmas*, American Institute of Physics, ISBN 0883188597
- Sulaiman, A. H., Farrell, W. M., Ye, S. Y., Kurth, W. S., Gurnett, D. A., Hospodarsky, G. B., et al. (2019). A persistent, large-scale, and ordered electrodynamic connection between Saturn and its main rings. *Geophysical Research Letters*, *46*, 7166–7172. <https://doi.org/10.1029/2019GL083541>
- Sulaiman, A. H., Kurth, W. S., Hospodarsky, G. B., Averkamp, T. F., Persoon, A. M., Menietti, J. D., et al. (2018). Auroral hiss emissions during Cassini's Grand Finale: Diverse electrodynamic interactions between Saturn and its rings. *Geophysical Research Letters*, *45*, 6782–6789. <https://doi.org/10.1029/2018GL077875>
- Sulaiman, A. H., Kurth, W. S., Hospodarsky, G. B., Averkamp, T. F., Ye, S. Y., Menietti, J. D., et al. (2018). Enceladus auroral hiss emissions during Cassini's Grand Finale. *Geophysical Research Letters*, *45*, 7347–7353. <https://doi.org/10.1029/2018GL078130>
- Sulaiman, A. H., Kurth, W. S., Persoon, A. M., Menietti, J. D., Farrell, W. M., Ye, S. Y., et al. (2017). Intense harmonic emissions observed in Saturn's ionosphere. *Geophysical Research Letters*, *44*, 12,049–12,056. <https://doi.org/10.1002/2017GL076184>
- Szalay, J. R., Allegrini, F., Bagenal, F., Bolton, S. J., Bonfond, B., Clark, G., et al. (2020). Alfvénic acceleration sustains Ganymede's footprint tail aurora. *Geophysical Research Letters*, *47*, e2019GL086527. <https://doi.org/10.1029/2019GL086527>

- Szalay, J. R., Bagenal, F., Allegrini, F., Bonfond, B., Clark, G., Connerney, J. E. P., et al. (2019). Proton acceleration by Io's Alfvénic interaction. *Journal of Geophysical Research: Space Physics*, *125*, 1. <https://doi.org/10.1029/2019JA027314>
- Szalay, J. R., Bonfond, B., Allegrini, F., Bagenal, F., Bolton, S., Clark, G., et al. (2018). In situ observations connected to the Io footprint tail aurora. *Journal of Geophysical Research: Planets*, *123*, 3061–3077. <https://doi.org/10.1029/2018JE005752>
- Szalay, J. R., Allegrini, F., Bagenal, F., Bolton, S. J., Bonfond, B., Clark, G., et al. (2020). A new framework to explain changes in Io's footprint tail electron fluxes: A new framework to explain changes in Io's footprint tail electron fluxes. *Geophysical Research Letters*, *47*, e2020GL089267. <https://doi.org/10.1029/2020GL089267>
- Tetrick, S. S., Gurnett, D. A., Kurth, W. S., Imai, M., Hospodarsky, G. B., Bolton, S. J., et al. (2017). Plasma waves in Jupiter's high-latitude regions: Observations from the Juno spacecraft. *Geophysical Research Letters*, *44*, 4447–4454. <https://doi.org/10.1002/2017GL073073>
- Xin, L., Gurnett, D. A., Santolík, O., Kurth, W. S., & Hospodarsky, G. B. (2006). Whistler-mode auroral hiss emissions observed near Saturn's B ring. *Journal of Geophysical Research*, *111*, A6. <https://doi.org/10.1029/2005JA011432>

References From the Supporting Information

- Kolmašová, I., Imai, M., Santolík, O., Kurth, W. S., Hospodarsky, G. B., Gurnett, D. A., et al. (2018). Discovery of rapid whistlers close to Jupiter implying lightning rates similar to those on Earth. *Nature Astronomy*, *2*(7), 544–548. <https://doi.org/10.1038/s41550-018-0442-z>